Shape-Stabilized Phase Change Materials: Performance of Simple Physical Blending Synthesis and the Potential of Coconut Based Materials

Ahmad Rifqi Muchtar, Christopher Hassam, Bhuvanesh Srinivasan, David Berthebaud, Takao Mori, Nugroho Soelami, Brian Yuliarto

Shape-Stabilized Phase Change Materials: Performance of Simple Physical Blending Synthesis and the Potential of Coconut Based Materials

Ahmad Rifqi Muchtar,[ab] Christopher L. Hassam,[bc] Bhuvanesh Srinivasan,[bc] David Berthebaud,[c]* Takao Mori,[b]* Nugroho Soelami,[ad] Brian Yuliarto[ae]*

a. Institut Teknologi Bandung (ITB), Department of Engineering Physics, Jalan Ganesha 10, Bandung, 40132 Indonesia.
b. National Institute for Materials Science (NIMS), WPI International Center for Materials Nanoarchitectonics (WPI-MANA), 1-1 Namiki, Tsukuba, 305-0044 Japan.
c. CNRS-Saint Gobain-NIMS, IRL 3629, LINK, National Institute for Materials Science (NIMS), 1-1 Namiki, Tsukuba, 305-0044 Japan.
d. Building Physics Research Group, Faculty of Industrial Technology, Institut Teknologi Bandung (ITB), Jalan Ganesha 10, Bandung 40132, Indonesia.
e. Advanced Functional Materials Research Group, Faculty of Industrial Technology, Institut Teknologi Bandung (ITB), Jalan Ganesha 10, Bandung, 40132 Indonesia.

** Corresponding authors: David.BERTHEBAUD@cnrs.fr; MORI.Takao@nims.go.jp; brian@tf.itb.ac.id*

Abstract

This research reports, for the first time, the combination of food-grade coconut oil and coconut shell-based activated carbon as precursors for the synthesis of bio-based shape-stabilized phase change materials (bioSSPCM). Despite its low melting enthalpy, simple physical blending by heating and mixing is found to be a very reliable preparation method for the completely coconut-based materials, producing a thermally stable bioSSPCM with anti-leakage. No difference between food grade and analytical grade coconut oil, in terms of its application for SSPCMs, was evident. Further, comparing the performance of coconut oil against octadecane, a conventional phase change material, it was found that with the same synthesis conditions, the coconut oil exhibited improved stability, with less leakage after phase change cycling.

Keywords: Phase change materials; Coconut based-materials; Latent heat storage; Activated carbon; Buildings & thermal comfort

Introduction

In 2019 it was estimated that buildings consume 30-40% of global energy production and emit 38% of global energy-related CO_2 emission [1,2]. However, though energy consumption is common to all industrial, commercial, residential, and governmental buildings, the energy demands of each type vary differently, both throughout the day and throughout the year. Maintaining buildings for the thermal comfort of the occupants is necessary, and a great deal of energy is used in heating cold buildings at night and in cooling warm ones during the day. Storing thermal energy for later use is one method of reducing the energy demand for buildings, for example, by allowing heat to be stored during the day, enabling a house to be heated during the night.

In buildings, such thermal storage can be realized by the incorporation of latent heat storage materials into the building structure that could store and release heat while phase changing. Materials suited to this are referred to as phase change materials (PCMs) [3–5]. For PCMs to be of use for thermal energy storage in buildings, the phase change must occur within the correct temperature range, usually between 22 to 28 ^{o}C [6]. Many such PCMs in use are available whether euectic mixtures, inorganic materials including many low-melting

temperature salts, and organic materials, such as fatty acids and fossil fuel-derived waxes [7]. With the rapid depletion of fossil fuel sources throughout the world, relying on such waxes to attempt latent heat storage poses a problem with the ongoing viability of the method. Instead, the development of renewable and environmentally friendly PCMs should be emphasized. By using environmentally friendly materials with a melting temperature within the range of building comfort, electricity consumption could be reduced and waste heat repurposed; such applications have shown promise, especially in temperature peak shaving and shifting [8,9].

One obstacle for PCM applications in buildings is the leakage of the materials while in its liquid phase. There are multiple strategies to ensure that PCMs remain stabilized in a building structure; in particular, encapsulation (microencapsulation or macroencapsulation) [3,10–12] and shape stabilization [13–15] are two well-known methods. The encapsulation techniques are well developed [16], and now various commercial products in the form of micro or macro encapsulated PCMs are available [17]. Shape stabilization also shows considerable progress for potential applications [8]. Comparatively, though microcapsule PCMs are possible to be used for latent energy storage in buildings, the practical application of them becomes prohibitively expensive, due to the relatively large quantity of PCMs required for a typical building. Due to this, less expensive materials and synthesis methods must be further developed.

Shape-stabilized phase change materials (SSPCMs) use the porous structure of a material to support the PCM and prevent leakage whilst in its liquid form. Three categories of nanoscale pores are defined by IUPAC [18], and of these, it was reported that the mesopores and micropores are more preferable for SSPCM due to optimal surface tension and capillary forces [19]. Activated carbon is an organic-based material that has been studied as the supporting structure for PCMs because of its high specific surface area and porosity [20,21]. The use of activated carbon as the supporting structure could increase the thermal conductivity of the SSPCM [22–24].

Biomass activated carbon is an environmentally friendly material that can be used as the SSPCM supporting structure, and critically, can be produced in low cost, and environmentally friendly ways. Kim et al. reported that the production of one kilogram of activated carbon from wood waste is capable of reducing global warming potential (GWP) by about 10 kg CO2-eq compare to coal based activated carbon, and the use of one ton of wood waste for activated carbon can reduce the GWP by 163 kg CO2-eq compared to wood waste landfill [25]. The shell of coconut which is a by-product of coconut water,milk and oil production has becomes a biomass waste problem, especially in tropical countries [26]. This agricultural waste product will be present for as long as the demand for coconuts and coconut products exist. In 2020 alone it was estimated that the global coconut production was 62.5 million tons, with demand set to increase in the coming years [27,28]. The use of biomas waste product for activated carbon sources will not just lower the cost of material, but simultaneously will reduce the cost of dealing with an existing waste product. Food grade coconut oil and activated carbon are already common market products, which means an established production/synthesis procedure and inexpensive price. Adding to that, the use of a simple synthesic method such as avoiding the use of solvents and vacuum for SSPCM fabrication will lower the cost even more.

Many reports investigate the use of activated carbon as a supporting material for organic PCMs; some examples are listed in Table 1. Octadecane as a paraffin compound with high latent heat has been widely researched for thermal comfort applications. Octadecane has also been mixed with biomass-based activated carbon such as palm kernel [29,30], and peat soil [31]. Despite its high latent heat, octadecane is mostly produced from the refinery process of natural gas (which is non-renewable) and hence relatively expensive. On top of the use of biomass-activated carbon, using organic PCMs, especially bio-based PCMs will increase its

environmentally friendly nature. Fatty acid SSPCMs, using palmitic acid [22,32], stearic acid [23,24], and lauric acid [33] have been successfully prepared with activated carbon acting as the supporting structure. Fewer reports are found about the combination of biomass-based activated carbon with renewably sourced PCMs [34,35], but it is undoubtedly a worthwhile effort to achieve more environmentally sustainable materials with an additional economic incentive in the form of simultaneous elimination of an existing waste product.

For preparation, commonly bioSSPCM are made by physical blending using solvents or by vacuum impregnation. These two methods have shown their potential to produce SSPCMs with a PCM loading capacity of over 90% by weight [32,34,36] and retain a melting enthalpy of over 95% compared to its pure PCM counterpart [23,24,37]. Nevertheless, the need for solvents, filtering, and vacuum processes translate to higher production costs and environmental impact. To assess the SSPCM, besides the typical material and thermal characterization, a leakage test is unavoidable to confirm the ability of the supporting structure to retain the PCM in its structure. Heating on paper is the most favoured method, as can be seen in Table 1.

In this study coconut-based PCMs were examined, using a simple physical blending method to produce an inexpensive, eco-friendly, and high-performing bioSSPCM, using abundant and easily obtained materials. Coconut oil is a commonly used product that has a melting point near room temperature, hence the potential for maintaining thermal comfort. To stabilize the liquid form, the coconut oil will be supported by activated carbon synthesized from coconut shells. This combination of coconut oil and coconut shell is a novel bioSSPCM, that has the potential as a passive thermoregulator in buildings, especially in tropical countries with abundant production of coconut palms, and as a side note also a way to solve the problem of large coconut shell waste. Two different types of coconut oil (market and analytical grade) were used to investigate if any effect of processing impacts upon the performance for SSPCM applications. To further understand the effect of the simple physical blending synthesis for different types of organic PCM and activated carbon, octadecane as a PCM and two other types of activated carbon as supporting structures were investigated. As illustrated in Fig.1, despite the low latent heat compared to octadecane, this work investigates the advantages of using coconut-based materials for SSPCMs by simple physical blending synthesis. To our knowledge, this research is the first that reports on the combination of coconut oil and coconut shell-based activated carbon as a bioSSPCM.

Materials and methods

Materials

Steam-activated carbon made from coconut shells, Y-180C (AC_{steam}) was obtained from Ajinomoto Fine-Techno Inc., food-grade organic virgin coconut oil (CO_{food}) was purchased and used without additional purification. Basic and neutral analytical grade charcoal-based activated carbon (AC_{basic} and $AC_{neutral}$) and analytical grade (1^{st} grade) coconut oil were obtained from Wako Chemical Inc. (CO_{an}), and analytical grade octadecane (99%) was purchased from Sigma Aldrich (Oct). All the materials used in this experiment were used directly without prior treatment. The photographs of all the precursors used in this experiment are shown in SI Fig. S1 and Fig. S2.

SSPCM Synthesis

The SSPCM samples were prepared by simple physical blending synthesis, as illustrated in Fig. 2. In a typical preparation, specific amounts of PCM and activated carbon (for the range of

values studied, please refer to SI Loading capacity check) were heated up to 80 ^{o}C and held for 10 minutes, then the activated carbon was poured into the liquid PCM and stirred for 10 minutes. The resultant material from this process is the shape-stabilized phase change material (SSPCM), used for further analysis. Approximately 3 g of the resulting material was then shaped into a cylinder using a 10 mm diameter metal die-piston set (SI Fig. S3). Before fabricating the SSPCM samples, the PCM optimal ratios were determined by varying the quantity of activated carbon to PCM for samples (SI Loading capacity check). Unless otherwise described, measurements in this work use the determined optimal ratios, 1:0.8 AC_{steam}:PCM, 1:1.8 AC_{basic}:PCM, and 1:1.2 $AC_{neutral}$:PCM.

Characterization

X-Ray Diffraction (XRD) patterns were taken with a Rigaku Smart Lab 3 diffractometer (Cu radiation, $\lambda_{K\alpha1}$ = 1.5418 Å, and $\lambda_{K\alpha2}$= 1.5444 Å), across a range of 10^{o}-90^{o} with a step width of 0.02^{o} at a scan speed of 8^{o}. Fourier Transform Infra-Red (FTIR) spectra were obtained using a Shimadzu IRAffinity-1S in the range of 500-4000 cm^{-1}. Scanning Electron Microscopy (SEM) images were taken with a Hitachi S-4800 with an accelerating voltage of 10 kV. Using data from the nitrogen adsorption isotherm (BELSORP-mini II Sorption System), surface areas were calculated by the Brunauer-Emmett-Teller (BET) method, and pore diameter and pore volume were calculated by Barrett-Joyner-Halenda (BJH) method. Thermogravimetric analysis (TGA) was conducted using a Hitachi TG/DTA6200 with a 20 ^{o}C/min heating rate under nitrogen flow 20 ml/min. Differential Scanning Calorimetry (DSC) was conducted using a Hitachi X-DSC7000 at a 5 ^{o}C/min heating rate. From DSC measurement, melting temperatures (T_m) were determined and melting enthalpies (ΔH_m) were calculated. Theoretical melting enthalpies (ΔH_{m-T}) were calculated according to equation (ΔH_{m-T} = ΔH_m x loading capacity). Thermal diffusivities (α) were measured by a Laser Flash Technique with a Netzsch LFA 467-HT at room temperature using a specialized sample holder. The thermal conductivities (κ) were calculated according to equation ($\kappa = \alpha . C_p . \rho$), where C_p is specific heat (obtained from DSC measurement) and ρ is the density at room temperature. Leakage testing was done by heating the samples above a filter paper, from room temperature up to ~75 ^{o}C and maintaining the elevated temperature for 30 minutes. Sample masses were taken before and after the heating process. A Testo 868 instrument was used to take the infra-red and real images of the SSPCM samples at four temperature points while conducting the leakage test.

Result and discussion

The preliminary experiment concluded that the optimal loading capacities of the PCM into activated carbon (SI Fig. S3b and 3d) are 80%, 180%, and 120% of mass for AC_{steam}, AC_{basic}, and $AC_{neutral}$, respectively. It was found that the loading capacity is the same regardless of PCM type. From the three types of activated carbon and three types of PCM, nine SSPCM samples were prepared, as shown in Table 2.

XRD and FTIR analysis

The XRD patterns of the three activated carbon precursors (Fig. 3a) show broad peaks at 24^{o} and 43^{o}, which belong to the (002) and (100) planes, respectively [13,23]. The graphite crystal phase at 26.5^{o} (002 plane) was also observed on the $AC_{neutral}$ compared to the other two activated carbon [38]. This indicates that the three activated carbon are largely amorphous whilst $AC_{neutral}$ contains some graphite crystals. The coconut oil samples show a broad peak at 20^{o,} indicating the amorphous phase of polymer, similar to the reported pattern by other [39], and no significant difference between CO_{food} and CO_{an} pattern was observed. The Oct pattern

shows the β-form crystal phase of *n*-octadecane at 19.2^{o} (010), 19.7^{o} (011), 24.5^{o} (-101), and 24.6^{o} (110) and the α-form crystal phase of n-octadecane at 11.5^{o} (003), 15.3^{o} (004), 39.5^{o} (022), and 44.4^{o} (207) [10]. With this, the difference between the amorphous phase of coconut oil and the crystalline phase of octadecane was confirmed.

In the FTIR spectra Fig. 3b, the CO_{food} and CO_{an} display absorbencies at 2960 cm^{-1}, 2921 cm^{-1}, and 2854 $cm^{-1,}$ which indicates the sp^3 -CH stretching vibration, at 1742 cm^{-1} indicating the C=O stretching vibration, at 1466 cm^{-1} indicating the sp^3 -CH bending vibration, 1160-1109 cm^{-1} assigned to the acyl ester C-O vibration, and at around 720 cm^{-1} due to the -CH_2 rocking vibration [34,35]. The Oct spectrum shows peaks at 2913 cm^{-1} and 2848 cm^{-1} corresponding to the stretching vibrations of -CH_2 and -CH_3 groups respectively, at 1466 cm^{-1} and 1369 $cm^{-1,}$ which belong to the bending vibrations of the -CH_2 and -CH_3 groups, and 716 cm^{-1} which indicates in-plane rocking vibration of the -CH_2 group [40,41]. The spectrum of activated carbon shows an increasing sloping trend towards lower wavenumbers, with recognizable absorbency peaks at 2360 cm^{-1} (-CH stretching vibration), 1565-1725 cm^{-1} (C=O stretching vibration), and 1000-1200 cm^{-1} (C-O stretching vibration) [37].

In the XRD patterns of the SSPCMs (Fig. 4a), peaks that belong to each precursor were observed. The peak of coconut oil at 20^{o} is observed instead of the peak of activated carbon at 24^{o} which is likely covered by the peak valley. The activated carbon peaks at 26.5^{o} and 43^{o} are observed in the SSPCM samples as well. An interesting fact is, in the XRD pattern of AC-Oct samples, the octadecane crystal peaks are not present. The possible explanation is the X-Ray caused the scattered particles of octadecane to melt [42], on top of heat conduction by the activated carbon. Coincidentally, the amorphous liquid octadecane has a broad peak at 20^{o} [43]. From the FTIR spectra of SSPCM samples (Fig. 4b), all the observable peaks belong to the PCMs instead of activated carbon. The existence of activated carbon is indicated by the sloping trend of the spectra. From the XRD pattern and FTIR spectra of SSPCM samples, there is no new peak present which indicates that the main interaction between the PCM and the activated carbon is physical interaction in the form of PCM absorption into the porous carbon.

Thermal stability and composition of SSPCM

Plots of the precursor TGA curves are displayed in Fig. 5a. One degradation step (evaporation) occurs at 115-250 ^{o}C for octadecane and 280-430 ^{o}C for both CO_{food} and CO_{an}. The desorption of water particles in all activated carbon precursors mainly happened below 75 ^{o}C, as indicated in Fig. 5a. At 470 ^{o}C the activated carbon loses a total of 9%, 8%, and 12% of weight for AC_{steam}, AC_{basic}, and $AC_{neutral,}$ respectively. It is also interesting to note that from around 60 ^{o}C, $AC_{neutral}$ already shows 2-3% difference of weight loss compared to the two other activated carbon.

The thermogravimetry result of the SSPCM samples are shown in Fig. 5b. The heating of activated carbon in the synthesis process successfully expelled the water content in the activated carbon, as there is no degradation below 100 ^{o}C observed for all SSPCM samples. All the SSPCM samples show one degradation step (evaporation), just like its PCM precursor. From this TGA result, it was confirmed that for thermal comfort application, all these SSPCM samples are thermally stable.

Besides checking thermal stability, the heating in TGA measurement is also needed to confirm the composition of the SSPCM. Table 3 summarize the composition of PCMs in the samples, comparing synthesis to TGA composition. The PCM components of each sample are almost the same between synthesis and TGA results with differences of 1-2 %. A 5% difference is observed on $AC_{neutral}$-Oct sample, which may be related to the weight loss of $AC_{neutral}$ that

happened after 80 ^{o}C. From this TGA composition result, it is confirmed that the simple physical blending synthesis method used in this experiment is highly reliable.

Textural and microstructure analysis

The nitrogen adsorption measurement was performed on the three activated carbon precursors and three representatives of the samples, as shown in Fig. 6a, and the corresponding BJH pore size distribution is shown in Fig. 6b. The AC_{steam} precursor was identified as a type I adsorption isotherm [18] in which a steep increase of N_2 adsorption happened at very low pressure followed by negligible increment afterward. This steep increase of N_2 corresponds to a very high degree of microporosity (ø < 2 nm) as detailed in the Fig. 6d, and the negligible increment afterward corresponds to a very low degree of mesoporosity (2 nm < ø < 50 nm) as detailed in Fig. 6c. The AC_{basic} and $AC_{neutral}$ precursors show a steep increase of N_2 adsorption followed by a sharp knee and then a slight gradual increase which resembles the combination of type I and type II adsorption isotherm. This indicates that the pore size distribution is dominated by micropores with a small quantity of mesopores and macropores (50 nm < ø < 1000 nm) as detailed in Fig. 6c. From the difference of AC_{steam} with AC_{basic} and $AC_{neutral}$ curve, it was determined that AC_{steam} has a higher degree of microporosity compared to AC_{basic} and $AC_{neutral}$.

The AC_{steam}-CO_{food}, AC_{basic}-CO_{an}, and $AC_{neutral}$-Oct curves are identified as type III adsorption isotherm which suggests that the material exhibits nonporous or macropores texture. The AC_{steam}-CO_{food} and AC_{basic}-CO_{an} samples show almost no N_2 adsorption in all pressure range, which indicate fully occupied pores by CO_{food} and CO_{an}. The $AC_{neutral}$-Oct shows a small increase of N_2 adsorption in high relative pressure, which is indicative of interstices between the $AC_{neutral}$-Oct particles.

Table 4 summarizes the BET and BJH calculation results for the activated carbon precursor. The higher calculated S_{BET} value of AC_{steam} compared to AC_{basic} and $AC_{neutral}$ affirms the notion of the highest degree of micropores in AC_{steam} that result in higher surface area. Further, based on the cumulative volume of pores, that AC_{basic} has the greatest, followed by $AC_{neutral}$ and then AC_{steam}, which is in line with the loading capacity result (AC_{basic} > $AC_{neutral}$ > AC_{steam}). The most common pore diameter of the activated carbons is below 2 nm, or microporous.

Fig. 7 provides SEM images of the activated carbon precursor and SSPCM samples. The AC_{steam}, AC_{basic}, and $AC_{neutral}$ show similar irregular forms of particles which is common for activated carbon, with small particles size below 1 μm while the larger particle observed were in the range of 5-10 μm. This variation particle size might affect the size of interstitial area but not related to the size of the pores. The size of The six CO_{food} and CO_{an}-based samples also show similarity in which we can observe the interconnected white glow from electron charging caused by the insulating nature of coconut oil. This interconnected white glow indicates interconnection between particles of SSPCM by the melted part of coconut oils, and also supports the nitrogen adsorption result on AC_{steam}-CO_{food} and AC_{basic}-CO_{an} samples that no interstices exist between the particles, hence the fully occupied pores. On the other hand, the three octadecane-based samples show similarity with the activated carbon precursor in which the particles are separated, which is highly likely caused by octadecane's crystalline nature. This also explains the N_2 adsorption measurement on $AC_{neutral}$-Oct in which some macropores are detected which actually are the interstices between particles. This difference between the coconut oil and octadecane-based SSPCM samples further explains the difference between the amorphous and crystalline structure PCM and its effect when composed with amorphous carbon.

Comparing the N_2 adsorption measurement of AC_{steam}-CO_{food} and AC_{basic}-CO_{an} to the SEM results, it was determined that all CO_{food} and CO_{an}-based samples fully occupy the pores of the activated carbon. Despite the SEM images of octadecane-based samples showing similarity with its activated carbon precursors, however considering the N_2 adsorption measurement result of the $AC_{neutral}$-Oct sample and TGA results of all octadecane-based samples, it suggests that the octadecane also fully occupy activated carbon pores. This also accentuates the importance of loading capacity determination prior to actual sample synthesis.

Thermal storage and transport properties

The melting temperature (T_m) with its onset and offset melting temperature ($T_{m\text{-}on,}$ and $T_{m\text{-}off}$ respectively) of the SSPCM samples are displayed in Fig. 8. These values were obtained from DSC measurement of the samples as shown in SI Fig. S5. From DSC measurement in SI Fig. S5 it was observed that CO_{an} showed multiple melting events, with a primary T_m at 22.0 ^oC and a secondary at 29.4 ^oC, caused by the inhomogeneity of the CO_{an} components. Comparatively, the CO_{an}-based SSPCMs showed a single melting event similar to that of CO_{food}-based samples, suggesting the homogenization of the PCM during the physical blending. In Fig. 8 it can be seen that T_m and $T_{m\text{-}off}$ of all coconut oil-based samples show similarity to the CO_{food}. However, it was observed that there is a slight increase of $T_{m\text{-}on}$ of the samples compared to CO_{food}, which means the addition of activated carbon caused the melting process to start at a slightly higher temperature. This slight increase of $T_{m\text{-}on}$ is most likely caused by the increase of thermal conductivity, which promotes heat conduction and results in a more homogenous melting process. Conversely, when there is no activated carbon in coconut oil, the heat conduction will be slower and cause an inhomogeneous melting process, *i.e.,* the outer area will melt faster compared to the inner area.

The T_m, $T_{m\text{-}on,}$ and $T_{m\text{-}off}$ values of octadecane that were measured are in agreement with the reported values [44,45]. The mixing of octadecane with activated carbon widen the $T_{m\text{-}on}$-$T_{m\text{-}off}$ range, with a significant increase of the $T_{m\text{-}off}$, and a slight decrease in $T_{m\text{-}on}$. The T_m of all octadecane-based samples also increases significantly when made into a composite. The slight decrease in $T_{m\text{-}on}$ phenomena is quite the opposite of the coconut oil-based samples. Unlike the inhomogeneous melting process in coconut oil, the separate crystals of solid octadecane assure a higher surface area for heat exposure. The addition of activated carbon increases the thermal conductivity of the solid octadecane-based samples resulting in a faster start of the melting process, i.e., lower $T_{m\text{-}on}$. Once the octadecane in the samples starts melting, the addition of activated carbons increases both T_m and $T_{m\text{-}off}$ values. The reason for this temperature increment is likely the same as the reason for the increment of $T_{m\text{-}on}$ in coconut oil-based samples.

The ΔH_m of the CO_{food} and CO_{an} measured are consistent with the melting enthalpy of coconut oil summarized by Kahwaji and White from various reports as 105 ± 11 J/g [46]. The ΔH_m of the Oct that was measured is also in agreement with other reported values [45,47]. From Table 5, it is evident that the ΔH_m of all SSPCM samples decreases compared to that of its PCM precursor. This decrease in ΔH_m is expected because any given SSPCM consists of PCM and activated carbon. Unlike the PCM, activated carbon does not act as latent heat storage, and hence has the direct effect of reducing the heat storage capacity. However, the addition of activated carbon is important to improve the thermal conductivity and stability of PCM.

The measured melting enthalpy value (ΔH_m) was compared with the theoretical melting enthalpy ($\Delta H_{m\text{-}T}$) for a given SSPCM sample and the percentage of theoretical ($\Delta H_{\%}$) was calculated as a preliminary indicator of quality, resulting in values between 60-86% of $\Delta H_{m\text{-}T}$, as shown in Table 5. The sub-100% $\Delta H_{\%}$ performance of the composite materials was attributed to the effect of the pore size of activated carbon that causes i) limitation of the volume

of expansion while melting, hence limiting the absorbed latent heat, and ii) the unreachable pores under ambient pressure synthesis, leads to air pockets that were also limiting volume expansion of PCM. Nevertheless, this synthesis method resulting in $\geq$ 60% of $\Delta H_{\%}$ is satisfying - considering the simple and less expensive synthesis method.

To confirm the effect of activated carbon addition into the PCMs, four representative samples were selected, and the results compared to the thermal conductivity of the PCMs reported in the literature as shown in Fig. 9. The value of thermal conductivity of the coconut oil and octadecane were taken from the literature [34,48]. As expected, the addition of activated carbon increases the thermal conductivity of PCM, as has been reported for some organic-based SSPCMs such as fatty acids [22–24,33], PEG [36,49], and octadecane [37,48] as summarized in Table 1. In this experiment, the addition of activated carbon into coconut oil increased the thermal conductivity 31-44%, while the addition of activated carbon into the octadecane increased the thermal conductivity 32-52%.

Shape-Stabilize and Leakage Performance

The leakage phenomenon in SSPCMs is explainable by two physical parameters: i) microporosity which affects the capillary force of the PCM and ii) viscosity which affects the surface tension of the PCM. Both capillary force and surface tension will affect the flowability of PCM inside the carbon pores. The viscosity of coconut oil was reported to be 36 mPas and 7.6 mPas [50] and octadecane was reported to be 3.9 mPas and 1.6 mPas [51] at room temperature and 80 ^{o}C, respectively. Higher temperatures will increase the possibility of leakage; however, the capillary force caused by the micropore channels can prevent this leakage.

Fig. 10 shows the infra-red and actual image of the samples while heating, taken at some temperature points. After heating up to 75 ^{o}C and holding for 30 minutes, the cylindrical shape of all samples was retained and there was no leakage observed until 46 ^{o}C, which is already above the melting temperature of the samples. Observable in the last image in Fig. 10, after holding the samples at 75 ^{o}C for 30 minutes, the majority of SSPCM samples leave traces of seepage on the paper. The sample mass was measured before and after the heating and the mass loss was calculated, as shown in Table 6. Two samples (AC_{steam}-CO_{food} and AC_{steam}-CO_{an}) showed a good result with no leakage trace on the paper. All octadecane-based samples show leakage, especially AC_{steam}-Oct and $AC_{neutral}$-Oct with losses above 3% of the weight after the test. The other four coconut oil-based samples also showed leakage between 0.5%-1.5% of the mass.

The minimum leakage measured in AC_{steam}-CO_{food} and AC_{steam}-CO_{an} samples is caused by the high degree of microporosity of the AC_{steam} precursor, which causes high capillary force, and the relatively high viscosity of coconut oil, which prevents its outflow even above the melting point. On the other hand, despite the high degree of microporosity of AC_{steam}, leakage is observed in the AC_{steam}-Oct sample, which is caused by the low viscosity of octadecane. This low viscosity of octadecane also explains the leakage observed in AC_{basic}-Oct and $AC_{neutral}$-Oct samples, on top of the small number of macropores observed in AC_{basic} and AC_{steam} that gives lower capillary force.

Besides the leakage test, a simple three-cycles DSC measurement on CO_{food} and the AC_{steam}-CO_{food} samples were conducted to see the stability of the samples over time, as shown in SI Fig S6a and 6b. The 1st cycle of CO_{food} shows two melting peaks and two freezing peaks, and in the second and third cycle the melting peaks converge into one while the two freezing peaks stayed the same. The AC_{steam}-CO_{food} sample shows almost overlapped curve of the three cycles

with one melting and one freezing peak. From this measurement it could be concluded that activated carbon addition homogenize all the coconut oil component and converged the melting/freezing peak.

Conclusion

The abundant availability of coconut materials, especially in tropical countries, coupled with the simple fabrication method is economically promising and environmentally friendly. The coconut-based bioSSPCM was successfully synthesized by a simple physical blending method. The loading capacity of coconut shell-based activated carbon (AC_{steam}) is 44%, and after the intrusion of coconut oil into its pores, resulting in bioSSPCM with an enthalpy of 42.6 J/s which is 60% of its theoretical value. Despite its lower loading capacity and melting enthalpy, the coconut bioSSPCM has the advantage of anti-leakage performance and thermal stability on top of its abundant-inexpensive material and synthesis process. Besides, the addition of activated carbon increased the thermal conductivity, which promoted heat conduction for faster and homogenous thermal distribution. For the purpose of building comfort, the need for large amounts of SSPCM that translate to high cost could potentially be solved with this coconut-based bioSSPCM, and the anti-leakage property also means even lower cost (low maintenance). Further research regarding integration methods, mechanical, and safety will be needed. It was confirmed that there is no distinct difference between food grade and analytical grade coconut oil in terms of its application for SSPCM materials. Further, it was shown that the simple physical blending method is not suitable for octadecane-based SSPCMs, because of its crystallinity and low viscosity, preventing stability of the SSPCM.

Conflicts of interest

There are no conflicts to declare.

Acknowledgements

A.R.M. acknowledges that his doctoral study in ITB has been financially supported by Lembaga Pengelola Dana Pendidikan (LPDP), Ministry of Finance of Indonesia. A.R.M. acknowledges the NIMS-ICGP program for the Indonesia-Japan mobility grant. A.R.M thanks Dr. Muhammad Iqbal from ITB for analysis N_2-sorption. C.L.H and B.S. thank JSPS for the postdoctoral fellowships P21723 and P19720 respectively. T.M. acknowledges the funding from JSPS KAKENHI 19F19720 and JST-Mirai JPMJMI19A1.

Supporting Information (SI) available: Photos of precursors, die-set for sample cylinder-shaping, loading capacity check, and DSC measurement.

[1] P.P. Kumar, D.A. Santos, E.J. Braham, D.G. Sellers, S. Banerjee, M.K. Dixit, Punching above its weight: life cycle energy accounting and environmental assessment of vanadium microalloying in reinforcement bar steel, Environ. Sci. Process. Impacts. 23 (2021) 275–290. https://doi.org/10.1039/D0EM00424C.
[2] F. Mostafavi, M. Tahsildoost, Z. Zomorodian, Energy efficiency and carbon emission in high-rise buildings: A review (2005-2020), Build. Environ. 206 (2021) 108329. https://doi.org/10.1016/j.buildenv.2021.108329.
[3] W. Wang, H. Cao, J. Liu, S. Jia, L. Ma, X. Guo, W. Sun, A thermal energy storage composite by incorporating microencapsulated phase change material into wood, RSC Adv. 10 (2020) 8097–8103. https://doi.org/10.1039/C9RA09549G.
[4] Y. Cui, J. Xie, J. Liu, J. Wang, S. Chen, A review on phase change material application in building, Adv. Mech. Eng. 9 (2017) 1687814017700828. https://doi.org/10.1177/1687814017700828.
[5] F. Kuznik, D. David, K. Johannes, J.-J. Roux, A review on phase change materials integrated in building walls, Renew. Sustain. Energy Rev. 15 (2011) 379–391. https://doi.org/10.1016/j.rser.2010.08.019.
[6] L.F. Cabeza, A. Castell, C. Barreneche, A. de Gracia, A.I. Fernández, Materials used as PCM in thermal energy storage in buildings: A review, Renew. Sustain. Energy Rev. 15 (2011) 1675–1695. https://doi.org/10.1016/j.rser.2010.11.018.
[7] M. Thambidurai, K. Panchabikesan, K.M. N, V. Ramalingam, Review on phase change material based free cooling of buildings—The way toward sustainability, J. Energy Storage. 4 (2015) 74–88. https://doi.org/10.1016/j.est.2015.09.003.
[8] M. Frigione, M. Lettieri, A. Sarcinella, Phase Change Materials for Energy Efficiency in Buildings and Their Use in Mortars, Materials. 12 (2019) 1260. https://doi.org/10.3390/ma12081260.
[9] Eco-Efficient Materials for Mitigating Building Cooling Needs, Elsevier, 2015. https://doi.org/10.1016/C2014-0-02697-4.
[10] F. He, X. Wang, D. Wu, New approach for sol–gel synthesis of microencapsulated n-octadecane phase change material with silica wall using sodium silicate precursor, Energy. 67 (2014) 223–233. https://doi.org/10.1016/j.energy.2013.11.088.
[11] A. Marani, M.L. Nehdi, Integrating phase change materials in construction materials: Critical review, Constr. Build. Mater. 217 (2019) 36–49. https://doi.org/10.1016/j.conbuildmat.2019.05.064.
[12] L. Royon, L. Karim, A. Bontemps, Optimization of PCM embedded in a floor panel developed for thermal management of the lightweight envelope of buildings, Energy Build. 82 (2014) 385–390. https://doi.org/10.1016/j.enbuild.2014.07.012.
[13] D.G. Atinafu, W. Dong, C. Wang, G. Wang, Synthesis of porous carbon from cotton using an $Mg(OH)_2$ template for form-stabilized phase change materials with high encapsulation capacity, transition enthalpy and reliability, J. Mater. Chem. A. 6 (2018) 8969–8977. https://doi.org/10.1039/C8TA01672K.
[14] Y. Li, L. Zhao, H. Wang, B. Li, Synthesis of novel shape-stabilized phase change materials with high latent heat and low supercooling degree for thermal energy storage, J. Mater. Res. 34 (2019) 3263–3270. https://doi.org/10.1557/jmr.2019.97.
[15] X. Min, M. Fang, Z. Huang, Y. Liu, Y. Huang, R. Wen, T. Qian, X. Wu, Enhanced thermal properties of novel shape-stabilized PEG composite phase change materials with radial mesoporous silica sphere for thermal energy storage, Sci. Rep. 5 (2015) 12964. https://doi.org/10.1038/srep12964.
[16] A. Sivanathan, Q. Dou, Y. Wang, Y. Li, J. Corker, Y. Zhou, M. Fan, Phase change materials for building construction: An overview of nano-/micro-encapsulation, Nanotechnol. Rev. 9 (2020) 896–921. https://doi.org/10.1515/ntrev-2020-0067.

[17] S.E. Kalnæs, B.P. Jelle, Phase change materials and products for building applications: A state-of-the-art review and future research opportunities, Energy Build. 94 (2015) 150–176. https://doi.org/10.1016/j.enbuild.2015.02.023.
[18] M. Thommes, K. Kaneko, A.V. Neimark, J.P. Olivier, F. Rodriguez-Reinoso, J. Rouquerol, K.S.W. Sing, Physisorption of gases, with special reference to the evaluation of surface area and pore size distribution (IUPAC Technical Report), Pure Appl. Chem. 87 (2015) 1051–1069. https://doi.org/10.1515/pac-2014-1117.
[19] C. Li, H. Yu, Y. Song, M. Wang, Z. Liu, A n-octadecane/hierarchically porous TiO2 form-stable PCM for thermal energy storage, Renew. Energy. 145 (2020) 1465–1473. https://doi.org/10.1016/j.renene.2019.06.070.
[20] X. Tong, N. Li, M. Zeng, Q. Wang, Organic phase change materials confined in carbon-based materials for thermal properties enhancement: Recent advancement and challenges, Renew. Sustain. Energy Rev. 108 (2019) 398–422. https://doi.org/10.1016/j.rser.2019.03.031.
[21] A.F. Nicholas, M.Z. Hussein, Z. Zainal, T. Khadiran, Activated Carbon for Shape-Stabilized Phase Change Material, in: Synth. Technol. Appl. Carbon Nanomater., Elsevier, 2019: pp. 279–308. https://doi.org/10.1016/B978-0-12-815757-2.00013-9.
[22] Y. Wan, Y. Chen, Z. Cui, H. Ding, S. Gao, Z. Han, J. Gao, A promising form-stable phase change material prepared using cost effective pinecone biochar as the matrix of palmitic acid for thermal energy storage, Sci. Rep. 9 (2019) 11535. https://doi.org/10.1038/s41598-019-47877-z.
[23] C. Li, B. Xie, Z. He, J. Chen, Y. Long, 3D structure fungi-derived carbon stabilized stearic acid as a composite phase change material for thermal energy storage, Renew. Energy. 140 (2019) 862–873. https://doi.org/10.1016/j.renene.2019.03.121.
[24] B. Xie, C. Li, B. Zhang, L. Yang, G. Xiao, J. Chen, Evaluation of stearic acid/coconut shell charcoal composite phase change thermal energy storage materials for tankless solar water heater, Energy Built Environ. 1 (2020) 187–198. https://doi.org/10.1016/j.enbenv.2019.08.003.
[25] M.H. Kim, I.T. Jeong, S.B. Park, J.W. Kim, Analysis of environmental impact of activated carbon production from wood waste, Environ. Eng. Res. (n.d.) 10.
[26] R.K. Ahmad, S.A. Sulaiman, M. Inayat, H.A. Umar, The effects of temperature, residence time and particle size on a charcoal produced from coconut shell, IOP Conf. Ser. Mater. Sci. Eng. 863 (2020) 012005. https://doi.org/10.1088/1757-899X/863/1/012005.
[27] O. Azeta, A.O. Ayeni, O. Agboola, F.B. Elehinafe, A review on the sustainable energy generation from the pyrolysis of coconut biomass, Sci. Afr. 13 (2021) e00909. https://doi.org/10.1016/j.sciaf.2021.e00909.
[28] I.-F. Ignacio, T.-S. Miguel, Research opportunities on the coconut (Cocos nucifera L.) using new technologies, South Afr. J. Bot. 141 (2021) 414–420. https://doi.org/10.1016/j.sajb.2021.05.030.
[29] A.F. Nicholas, M.Z. Hussein, Z. Zainal, T. Khadiran, Palm Kernel Shell Activated Carbon as an Inorganic Framework for Shape-Stabilized Phase Change Material, Nanomaterials. 8 (2018) 689. https://doi.org/10.3390/nano8090689.
[30] A.F. Nicholas, M.Z. Hussein, Z. Zainal, T. Khadiran, The effect of surface area on the properties of shape-stabilized phase change material prepared using palm kernel shell activated carbon, Sci. Rep. 10 (2020) 15047. https://doi.org/10.1038/s41598-020-72019-1.
[31] M.Z. Hussein, T. Khadiran, Z. Zainal, R. Rusli, Properties of N-Octadecane-Encapsulated Activated Carbon Nanocomposite for Energy Storage Medium: The Effect of Surface Area and Pore Structure, Aust. J. Basic Appl. Sci. (2015) 8.

[32] M. Mehrali, S. Tahan Latibari, M.A. Rosen, A.R. Akhiani, M.S. Naghavi, E. Sadeghinezhad, H.S.C. Metselaar, M. Mohammadi Nejad, M. Mehrali, From rice husk to high performance shape stabilized phase change materials for thermal energy storage, RSC Adv. 6 (2016) 45595–45604. https://doi.org/10.1039/C6RA03721F.
[33] Z. Chen, F. Shan, L. Cao, G. Fang, Synthesis and thermal properties of shape-stabilized lauric acid/activated carbon composites as phase change materials for thermal energy storage, Sol. Energy Mater. Sol. Cells. 102 (2012) 131–136. https://doi.org/10.1016/j.solmat.2012.03.013.
[34] J. Jeon, J.H. Park, S. Wi, S. Yang, Y.S. Ok, S. Kim, Latent heat storage biocomposites of phase change material-biochar as feasible eco-friendly building materials, Environ. Res. 172 (2019) 637–648. https://doi.org/10.1016/j.envres.2019.01.058.
[35] J. Jeon, J.H. Park, S. Wi, S. Yang, Y.S. Ok, S. Kim, Characterization of biocomposite using coconut oil impregnated biochar as latent heat storage insulation, Chemosphere. 236 (2019) 124269. https://doi.org/10.1016/j.chemosphere.2019.06.239.
[36] D.-L. Feng, Y.-Y. Zang, P. Li, Y.-H. Feng, Y.-Y. Yan, X.-X. Zhang, Polyethylene glycol phase change material embedded in a hierarchical porous carbon with superior thermal storage capacity and excellent stability, Compos. Sci. Technol. 210 (2021) 108832. https://doi.org/10.1016/j.compscitech.2021.108832.
[37] T. Khadiran, M.Z. Hussein, Z. Zainal, R. Rusli, Shape-stabilised n-octadecane/activated carbon nanocomposite phase change material for thermal energy storage, J. Taiwan Inst. Chem. Eng. 55 (2015) 189–197. https://doi.org/10.1016/j.jtice.2015.03.028.
[38] N. Saafie, M.F.R. Samsudin, S. Sufian, R.M. Ramli, Enhancement of the activated carbon over methylene blue removal efficiency via alkali-acid treatment, AIP Conf. Proc. 2124 (2019) 020046. https://doi.org/10.1063/1.5117106.
[39] M. Xiao, L. Luo, B. Tang, J. Qin, K. Wu, F. Jiang, Physical, structural, and water barrier properties of emulsified blend film based on konjac glucomannan/agar/gum Arabic incorporating virgin coconut oil, LWT. 154 (2022) 112683. https://doi.org/10.1016/j.lwt.2021.112683.
[40] H. Li, X. Liu, G.-Y. Fang, Synthesis and characteristics of form-stable n-octadecane/expanded graphite composite phase change materials, Appl. Phys. A. 100 (2010) 1143–1148. https://doi.org/10.1007/s00339-010-5724-y.
[41] Y. Zhu, S. Liang, K. Chen, X. Gao, P. Chang, C. Tian, J. Wang, Y. Huang, Preparation and properties of nanoencapsulated n-octadecane phase change material with organosilica shell for thermal energy storage, Energy Convers. Manag. 105 (2015) 908–917. https://doi.org/10.1016/j.enconman.2015.08.048.
[42] A.J. Warren, D. Axford, R.L. Owen, Direct measurement of X-ray-induced heating of microcrystals, J. Synchrotron Radiat. 26 (2019) 991–997. https://doi.org/10.1107/S1600577519003849.
[43] S. Liang, Q. Li, Y. Zhu, K. Chen, C. Tian, J. Wang, R. Bai, Nanoencapsulation of n-octadecane phase change material with silica shell through interfacial hydrolysis and polycondensation in miniemulsion, Energy. 93 (2015) 1684–1692. https://doi.org/10.1016/j.energy.2015.10.024.
[44] J. Lee, S. Wi, S.-G. Jeong, S.J. Chang, S. Kim, Development of thermal enhanced n-octadecane/porous nano carbon-based materials using 3-step filtered vacuum impregnation method, Thermochim. Acta. 655 (2017) 194–201. https://doi.org/10.1016/j.tca.2017.06.013.
[45] F. He, X. Wang, D. Wu, New approach for sol–gel synthesis of microencapsulated n-octadecane phase change material with silica wall using sodium silicate precursor, Energy. 67 (2014) 223–233. https://doi.org/10.1016/j.energy.2013.11.088.

[46] S. Kahwaji, M.A. White, Edible Oils as Practical Phase Change Materials for Thermal Energy Storage, Appl. Sci. 9 (2019) 1627. https://doi.org/10.3390/app9081627.
[47] Y. Liu, Y. Xia, K. An, C. Huang, W. Cui, S. Wei, R. Ji, F. Xu, H. Zhang, L. Sun, Fabrication and characterization of novel meso-porous carbon/n-octadecane as form-stable phase change materials for enhancement of phase-change behavior, J. Mater. Sci. Technol. 35 (2019) 939–945. https://doi.org/10.1016/j.jmst.2018.11.001.
[48] T. Khadiran, M.Z. Hussein, Z. Zainal, R. Rusli, Activated carbon derived from peat soil as a framework for the preparation of shape-stabilized phase change material, Energy. 82 (2015) 468–478. https://doi.org/10.1016/j.energy.2015.01.057.
[49] L. Feng, J. Zheng, H. Yang, Y. Guo, W. Li, X. Li, Preparation and characterization of polyethylene glycol/active carbon composites as shape-stabilized phase change materials, Sol. Energy Mater. Sol. Cells. 95 (2011) 644–650. https://doi.org/10.1016/j.solmat.2010.09.033.
[50] T. Tipvarakarnkoon, R. Blochwitz, B. Senge, Rheological properties and phase change behaviors of coconut fats and oils, (n.d.) 7.
[51] M. Faden, S. Höhlein, J. Wanner, A. König-Haagen, D. Brüggemann, Review of Thermophysical Property Data of Octadecane for Phase-Change Studies, Materials. 12 (2019) 2974. https://doi.org/10.3390/ma12182974.

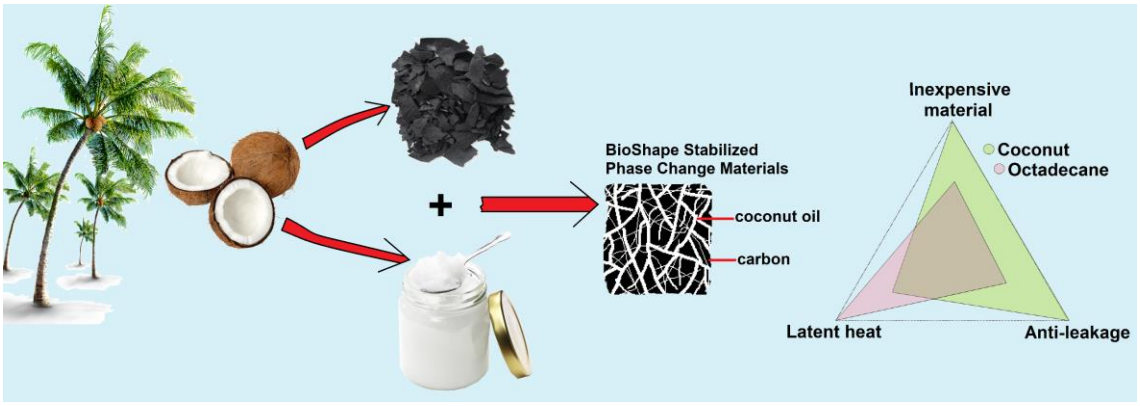

Fig. 1 Illustration of how coconut oil and coconut shell can be synthesized into shape stabilized phase change materials. The triangle diagram illustrating advantages and disadvantages of using coconut vs. octadecane for SSPCM material.

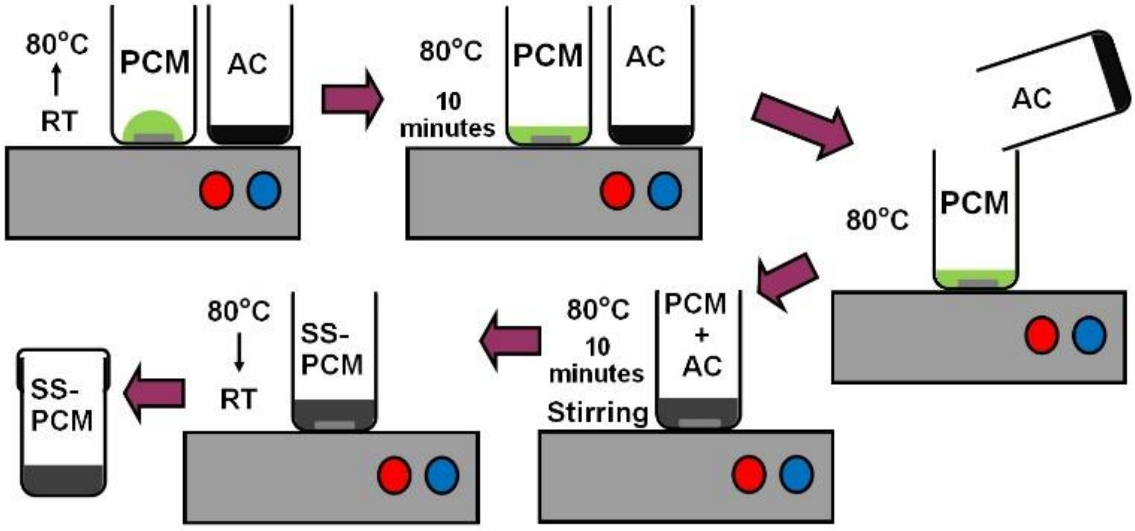

Fig. 2 Illustration of the simple physical blending synthesis of shape stabilized phase change materials.

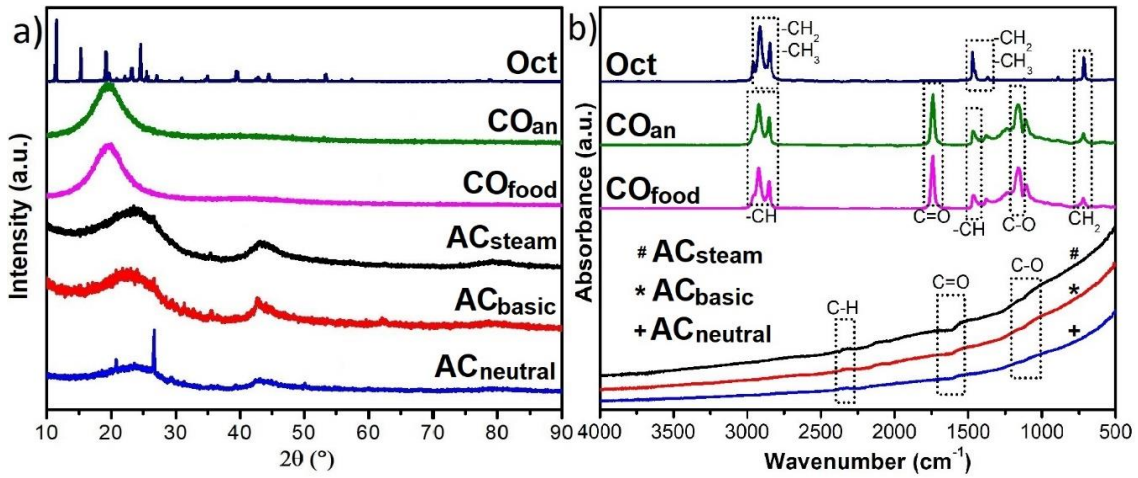

Fig. 3 (a) XRD patterns and (b) FTIR spectra of activated carbon and PCM prior to physical blending.

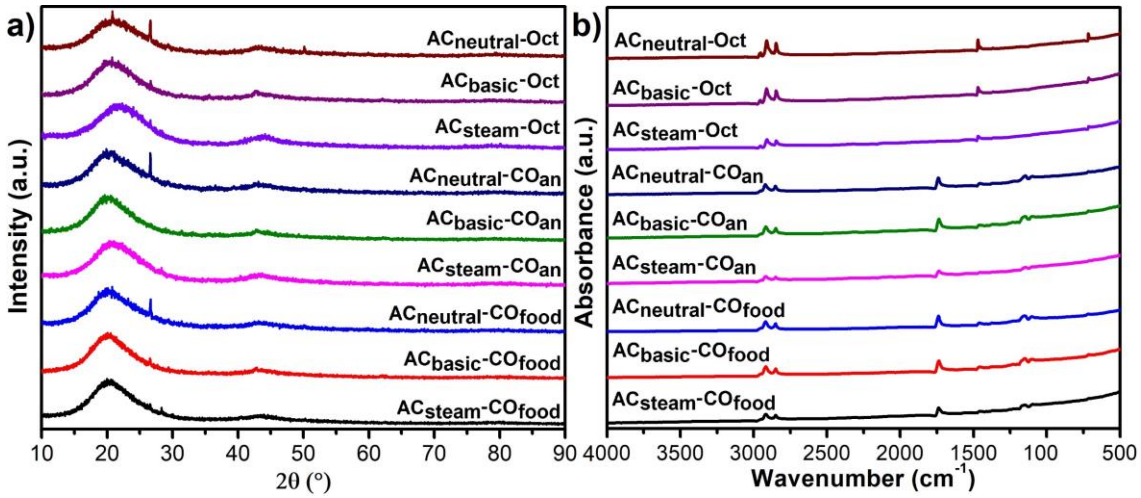

Fig. 4 (a) XRD patterns and (b) FTIR spectra of SSPCM samples after physical blending.

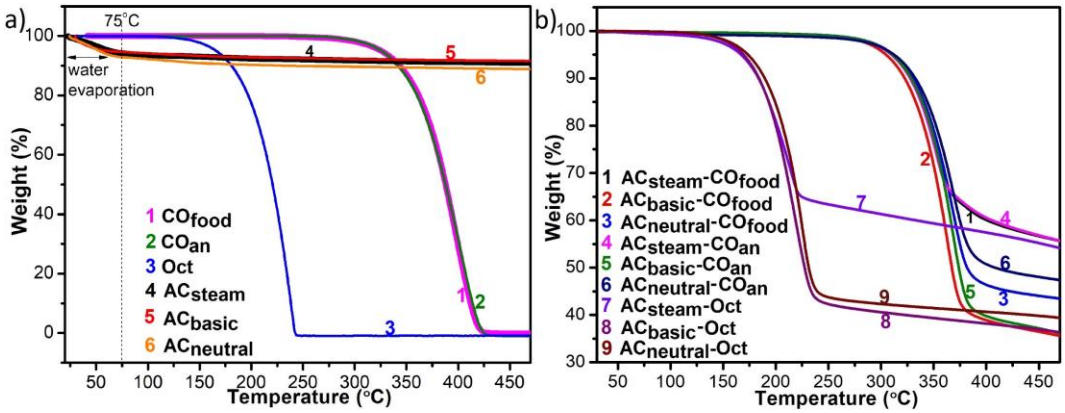

Fig 5. Thermogravimetry measurement on a) activated carbon and PCM precursor and b) SSPCM samples.

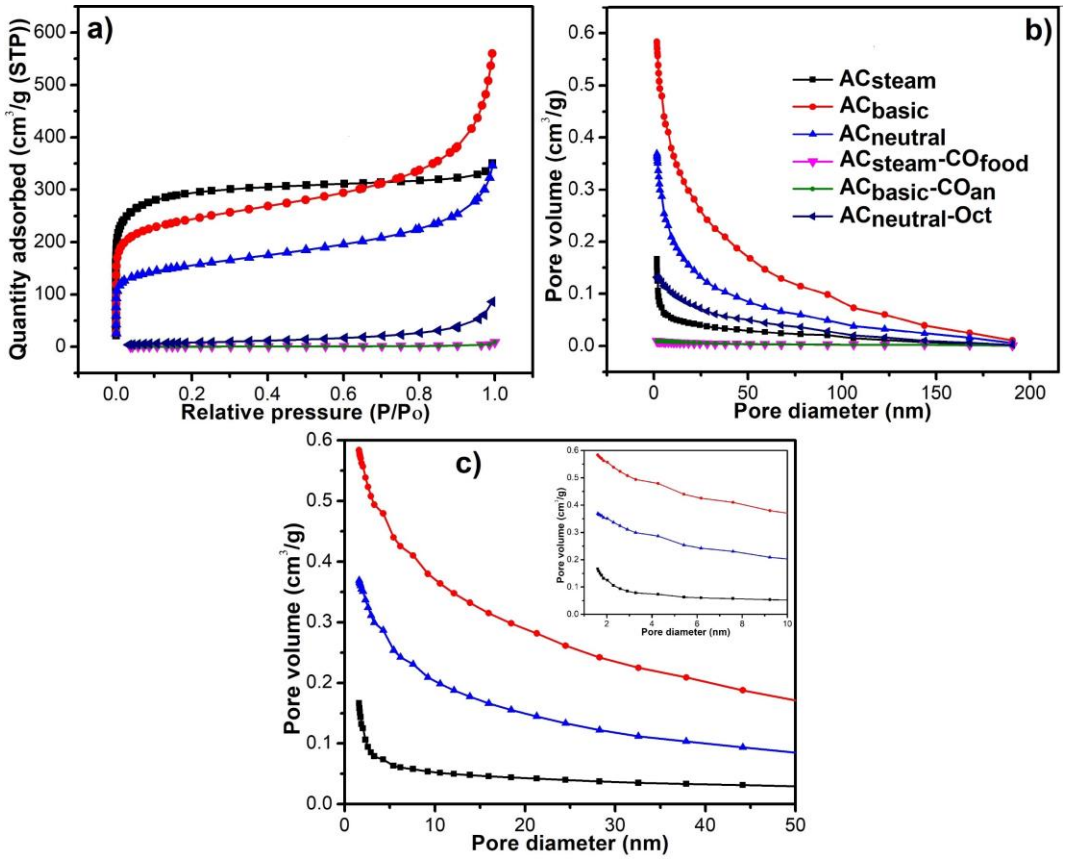

Fig. 6 (a) Nitrogen adsorption isotherm, (b) BJH pore size distribution for activated carbon and three SSPCM samples, and (c) 50 nm scale BJH pore size distribution, with inset in 10 nm scale

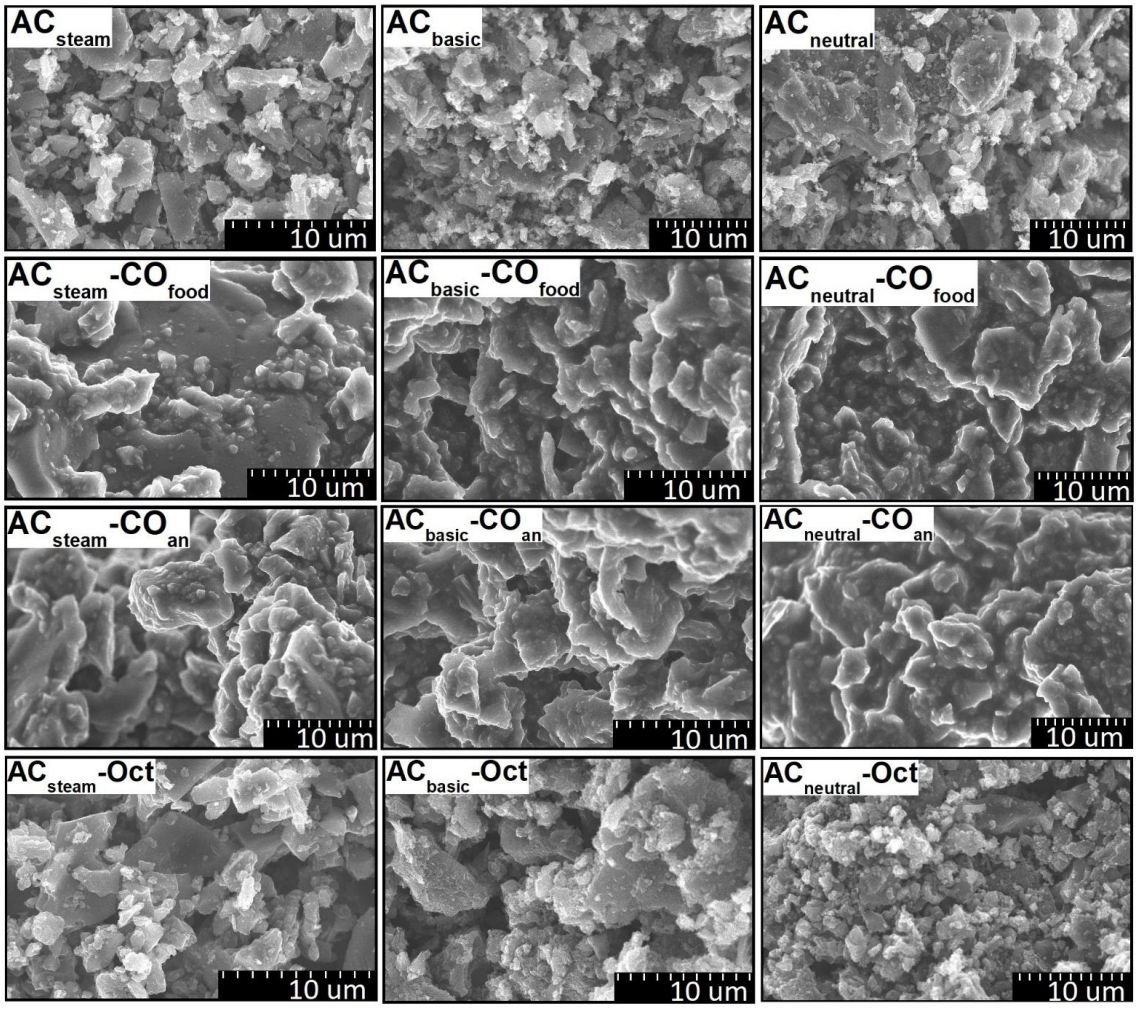

Fig 7. SEM images of precursor and SSPCM samples

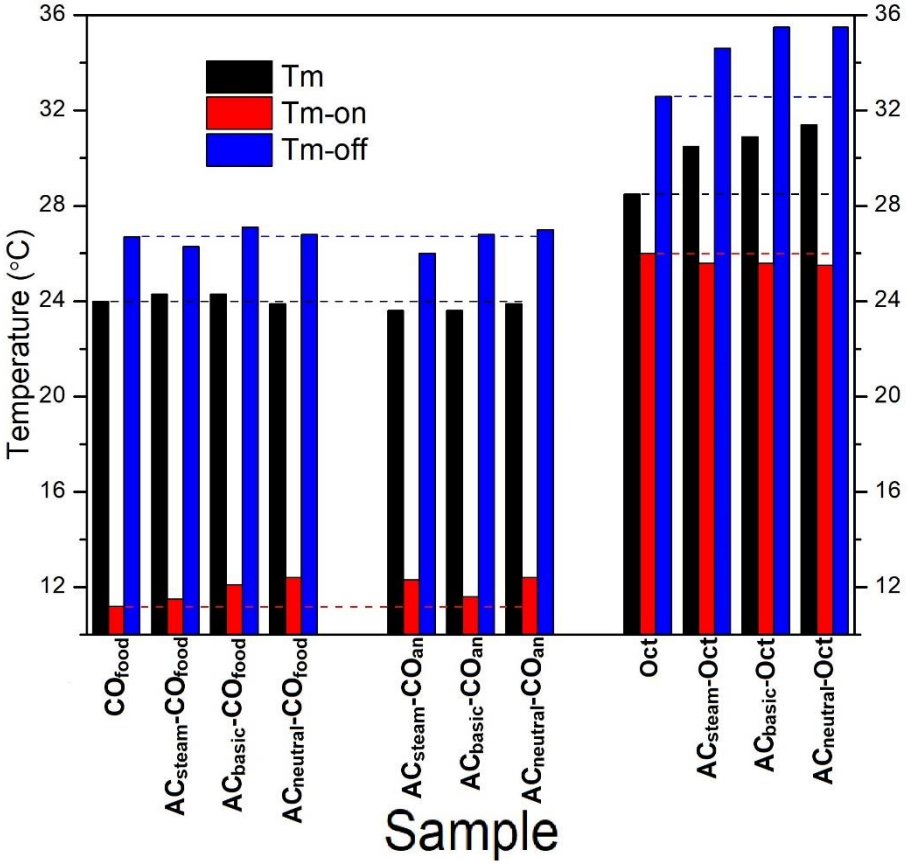

Fig. 8 The peak, onset, and offset melting temperature of PCM precursor and SSPCM samples.

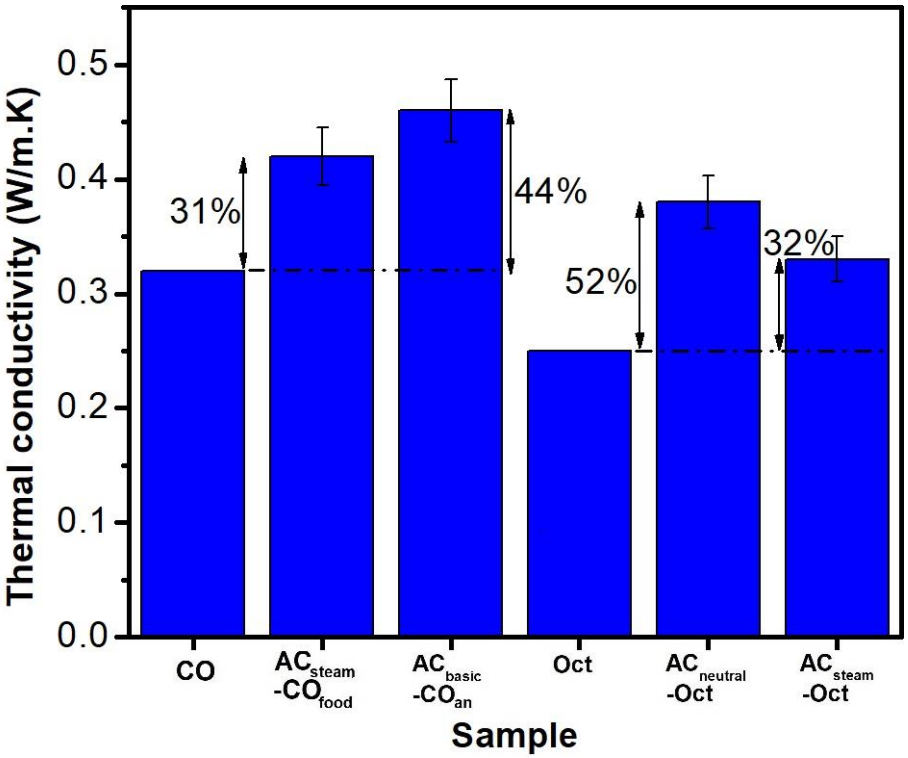

Fig. 9 Thermal conductivity of AC_{steam}-CO_{food}, AC_{basic}-CO_{an}, $AC_{neutral}$-Oct, and AC_{steam}-Oct. Error bar shows maximum possible standard deviation (6%).

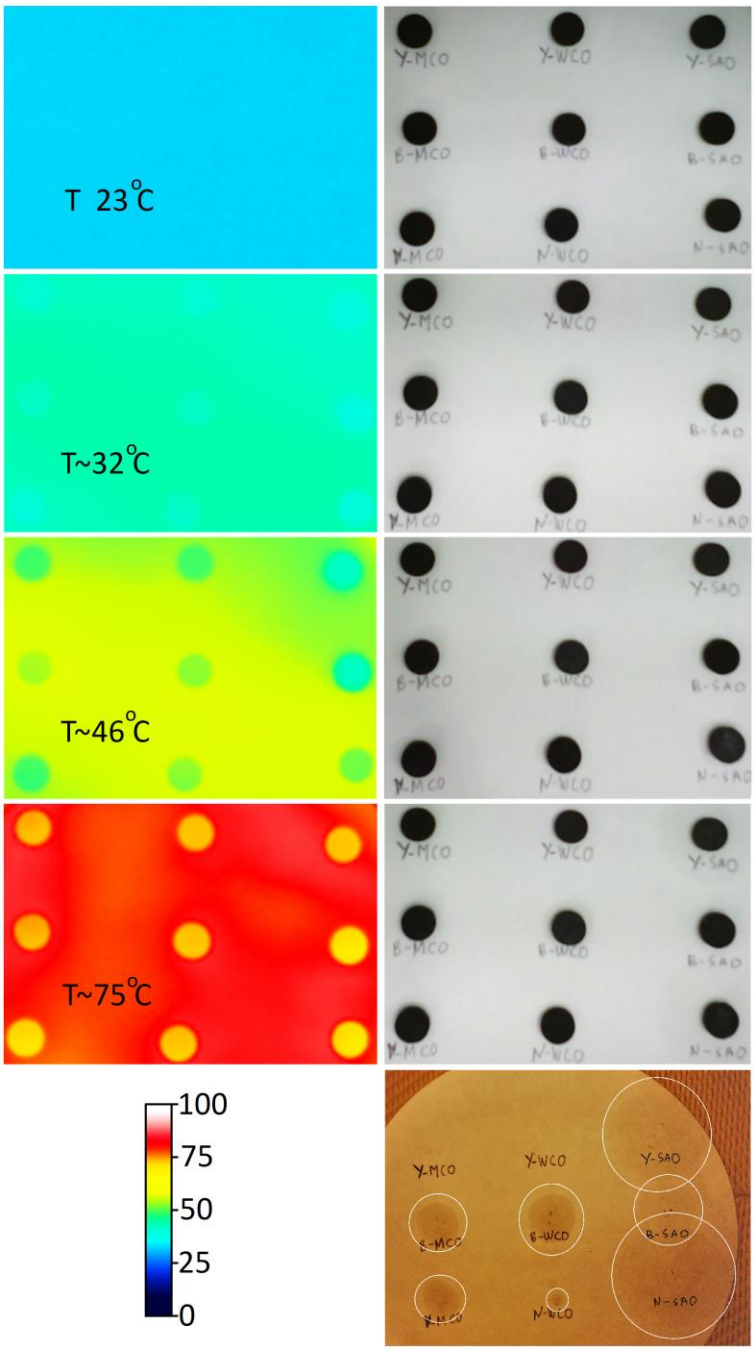

Fig. 10 Infra-red thermal imaging (left) and its actual photo (right). The last photo was taken directly after removing the samples, and then edited to clarify the absorbed PCM trace. (Y-MCO= AC_{steam}-CO_{food};Y-WCO= AC_{steam}-CO_{an};Y-SAO= AC_{steam}-Oct;B-MCO= AC_{basic}-CO_{food};B-WCO= AC_{basic}-CO_{an};B-SAO= AC_{basic}-Oct;N-MCO= $AC_{neutral}$-CO_{food};N-WCO= $AC_{neutral}$-CO_{an};N-SAO= $AC_{neutral}$-Oct)

Table 1 Summary of some organic based shape stabilized phase change materials

Activated carbon source	Organic PCM	Preparation method	PCM loading capacity	$\Delta H_{m\%}$	Leakage test method	Thermal conductivity (W/m.K)		Ref
						SSPCM	PCM	
Pinecone	Palmitic acid	Vacuum impregnation	60.0%	64.3%	Heating on paper	0.39	0.27	22
Rice husk	Palmitic acid	Vacuum impregnation	90.0%	96.1%	Heating without paper	0.28	0.28	31
Fungus (Esculenta)	Stearic acid	Vacuum impregnation	77.5%	97.5%	Heating on paper	0.57	0.27	23
Coconut shell	Stearic acid	Vacuum impregnation	35.3%	97.9%	Heating on paper	0.75	0.26	24
Commercial	Lauric acid	Physical blending	48.4%	74.8%	None	0.15	0.12	32
MOF-5	PEG2000	Physical blending with solvent	92.5%	90.6%	Heating on paper	0.31	0.33	23
Coconut shell	PEG6000	Physical blending with solvent	70.0%	58.6%	Not specified	-		36
Peat soil	Octadecane	Physical blending with solvent	47.4%	84.1%	Heating on paper	0.17	0.11	37
Commercial	Octadecane	Physical blending with solvent	45.0%	94.5%	Heating on paper	0.17	0.11	38
Rice husk	Coconut oil	Vacuum impregnation	80.0%	79.4%	Exudation stability	0.20	0.32	33

Table 2 The nine SSPCM samples obtained from mixing three PCMs by three activated carbons

Activated carbon	**PCM**		
	CO_{food}	**CO_{an}**	**Oct**
AC_{steam}	AC_{steam}-CO_{food}	AC_{steam}-CO_{an}	AC_{steam}-Oct
AC_{basic}	AC_{basic}-CO_{food}	AC_{basic}-CO_{an}	AC_{basic}-Oct
$AC_{neutral}$	$AC_{neutral}$-CO_{food}	$AC_{neutral}$-CO_{an}	$AC_{neutral}$-Oct

Table 3. %weight content of the precursor, comparison of the actual synthesis and TGA result

SSPCM sample	PCM content	
	Synthesis	TGA
AC_{steam}-CO_{food}	44%	44%
AC_{steam}-CO_{an}	44%	44%
AC_{steam}-Oct	44%	46%
AC_{basic}-CO_{food}	64%	64%
AC_{basic}-CO_{an}	64%	64%
AC_{basic}-Oct	64%	64%
$AC_{neutral}$-CO_{food}	55%	56%
$AC_{neutral}$-CO_{an}	55%	53%
$AC_{neutral}$-Oct	55%	60%

Table 4. Specific surface area calculated with BET method and pore properties calculated using BJH method

	S_{BET} (Specific surface area) (m^2/g))	BJH adsorption cumulative volume of pores (cm^3/g)	BJH adsorption frequent pore diameter (nm)
AC_{steam}	735.48	0.17	0.16
AC_{basic}	656.43	0.58	0.17
$AC_{neutral}$	430.13	0.37	0.17

Table 5. Melting enthalpy of PCM and SSPCM samples

SSPCM Samples	ΔH_m measured (J/g)	ΔH_m theoretical (J/g)	$\Delta H_{\%}$ (measured/theoretical) (J/g)
CO_{food}	96.8		
AC_{steam}-CO_{food}	25.5	42.6	60%
AC_{basic}-CO_{food}	41.3	62.9	66%
$AC_{neutral}$-CO_{food}	38.6	55.2	70%
CO_{an}	96.2		
AC_{steam}-CO_{an}	25.5	42.3	60%
AC_{basic}-CO_{an}	43.8	61.6	71%
$AC_{neutral}$-CO_{an}	34.4	51.0	67%
Oct	198.8		
AC_{steam}-Oct	62.0	91.4	68%
AC_{basic}-Oct	109.0	127.2	86%
$AC_{neutral}$-Oct	97.5	121.3	80%

Table 6. Sample mass decrease (in percent) after leakage testing

	CO_{food}	**CO_{an}**	**Oct**
AC_{steam}	0.17%	0.19%	3.84%
AC_{basic}	1.09%	1.52%	1.06%
$AC_{neutral}$	0.83%	0.54%	5.16%